Chapter 4

Cytocompatibility and osteogenic response

This chapter focuses on cytocompatibility and osteogenic activity of 1- and 2-D HA nanocrystals to evaluate the significant variation in their biological response. Additionally, the influence of morphology of HA nanocrystals on their surface oxygen vacancy, surface charge, and wettability is analyzed using XPS, zeta potential, and contact angle measurement, respectively. The variation in ion release behavior of HA nanocrystals is explained on the basis of their crystallinity. Further, the role of surface charge, hydrophilicity, ion release, and the size of different morphological HA nanocrystals on hemocompatibility, cell adhesion, proliferation, and differentiation is also thoroughly discussed.

4.1. Particle size and zeta potential measurement

To further verify the particle sizes of these nHA morphologies, Dynamic light scattering (DLS) particle size analyses were performed. Fig. 4.1A depicts the hydrodynamic size of HA nanorods, nanoplates, and thin nanoplates, which were measured to be 361 – 568 nm, 230 – 267 nm, and 768 – 1406 nm, respectively. The sizes of larger HA nanorods and thin nanoplates align well with FESEM results. However, the smaller particles might not appear in DLS particle size measurement due to agglomeration. The zeta potential measurement for HA nanorods, nanoplates, and thin nanoplates was also conducted to evaluate their surface charge and colloidal stability (Fig. 4.1 B). The zeta potential values were measured to be – 6.1, – 44.2 and – 48.1 mV for HA nanorods, nanoplates, and thin nanoplates, respectively. A higher negative zeta potential value indicates the minimum agglomeration in solutions due to repulsive force among the charged particles. It suggests good colloidal stability of HA nanoplates and thin nanoplates. It is well reported that the crystal structure of HA is such that the major exposed surface of HA nanorods is a (b)- crystallographic plane which is enriched with Ca^{2+} ions [1-3]. Therefore, the surface charge should be positive or less negative. In

contrast, the major exposed surface of HA nanoplates and thin nanoplates is c-plane, i.e., higher density of PO_4^{3-} and OH^- ions. Apparently, their surface charge should be negative or less positive. The zeta potential values for these HA samples align well with the crystallographic characteristics of HA.

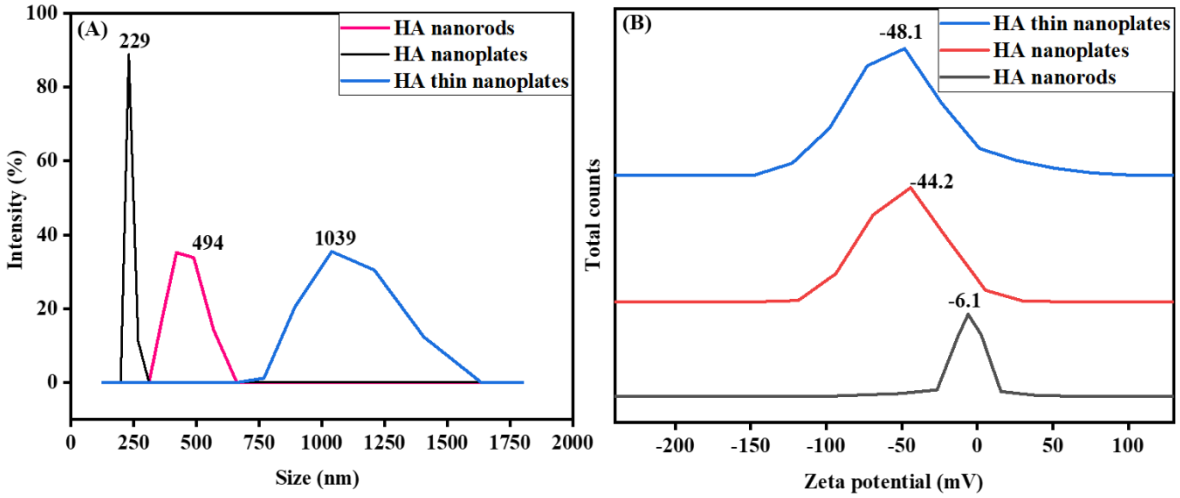

Figure 4.1. Particle size and surface charge assessment. *(A) DLS particle and (B) zeta potential plots of HA nanorods, nanoplates, and thin nanoplates.*

4.2. XPS analyses

Fig. 4.2 A (a – c) displays the survey XPS spectra of HA nanorods, nanoplates, and thin nanoplates where typically four types of elements: Ca2p, P2p, O 2p, and C1s are visible. The binding energy of C1s was observed at 284 eV, which is well-matched with the reported value [4, 5]. Based on the analyses of high-resolution individual peaks of Ca 2p and P 2p, it was deconvoluted into two predominant $2p_{3/2}$ and $2p_{1/2}$ peaks whose binding energies corresponded to (346.4, 350 eV) and (132.2, 133.4 eV) for HA nanorods, (346.3, 350 eV) and (132.1, 133 eV) for HA nanoplates, and (346.6, 350.3 eV) and (132.2, 133.4 eV) for HA thin nanoplates, respectively [5]. Three of them showed similar peak positions of Ca 2p and P 2p. In addition, the auger peaks of O KLL were also revealed.

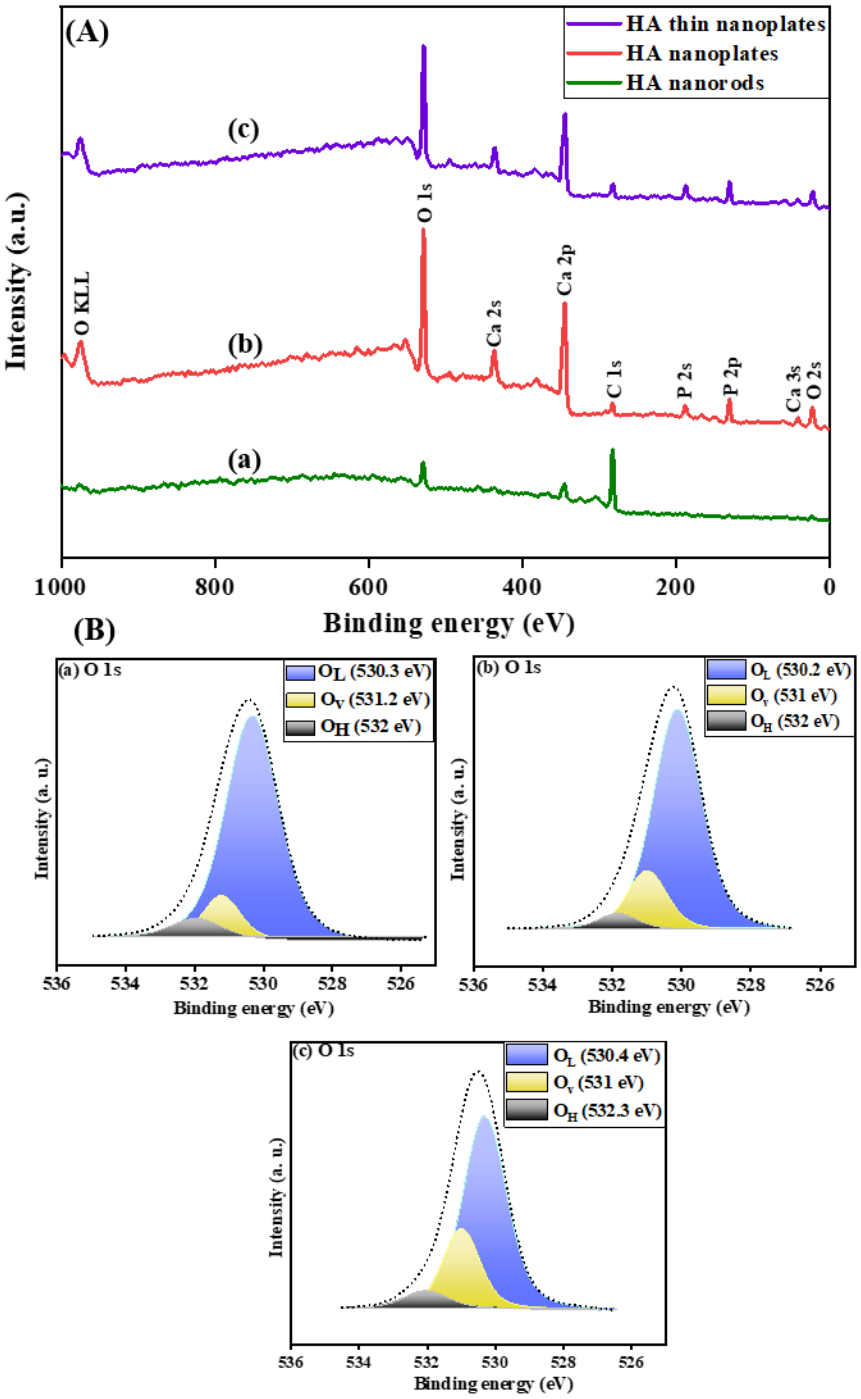

Figure 4.2. Surface chemistry analyses of different morphological HA nanocrystals. (A) *XPS survey spectra of HA nanorods (a), nanoplates (b), and thin nanoplates (c); (B) High resolution XPS spectra of O1s for HA nanorods (a), nanoplates (b), and thin nanoplates (c).*

The high-resolution analyses of XPS spectra of O 1s orbital for HA nanorods, nanoplates, and thin nanoplates were also performed (Fig. 4.2 B). The O 1s peak was deconvulated into three distinct peaks centered at binding energy of 530.3, 531.2 and 532 eV for HA nanorods, 530.2,

531 and 532 eV for HA nanoplates, and 530.4, 531 and 532.3 eV for HA thin nanoplates. The highest intense peaks of O 1s correspond to lattice oxygen (O_L), related to the P–O bond in all three nHA samples. Whereas the moderate intense peaks at 531 eV are attributed to adsorbed oxygen (O_{obs}) at O vacant sites, indicating the presence of O vacancy (O_V) in all three samples [6]**.** The ratio of adsorbed oxygen to lattice oxygen (O_{obs}/O_{latt}) provides the amount of surface oxygen vacancy on nHA samples [7]. It is clearly observed that the area of O_V peak increases as the morphology of HA nanocrystals changes from nanorods to nanoplates and nanoplates to thin nanoplates. Additionally, O_{obs}/O_{latt} was calculated to be 0.13, 0.22 and 0.35 for HA nanorods, nanoplates and thin nanoplates, respectively. It clearly reveals that HA thin nanoplates have higher concentrations of oxygen vacancies than HA nanorods and nanoplates. In the hexagonal crystal structure of HA, the a (b)-plane is enriched with Ca^{2+} ions, and the c-plane is enriched in PO_4^{3-} and OH^- ions, as already mentioned in the previous section. For a (b)-axis oriented HA nanoplates and c-axis oriented HA nanorods, the primary exposed surface is c-plane and a (b)-plane, respectively [1, 2]. Apparently, HA nanoplates with major exposed c-facet are more prone to forming oxygen vacancies due to the higher number of oxygen atoms on their surface than a (b)-facet. Previous studies suggest that the ease of oxygen vacancy formation is inversely proportional to the thickness of HA nanoplates [8, 9]. Consequently, the concentration of oxygen vacancies is higher in HA thin nanoplates. The smallest peaks (O_H) of HA nanorods, nanoplates and thin nanoplates are assigned to the surface hydroxyl (O–H) bond.

4.3. Ion leaching response

The concentration of Ca^{2+} and P^{5+} ions, leached from HA nanocrystals after immersion in SBF solution for 3, 5, and 7 days, are depicted in Fig. 4.3 A. Figs. 4.3 A (a) and (b) clearly indicate that the leaching of Ca^{2+} and P^{5+} ions from HA nanorods, nanoplates, and thin nanoplates increases continuously up to the concentrations of (3.034, 2.627 and 3.163 ppm) and (8.618, 7.075 and 8.911 ppm), respectively, over a period of 7 days. The leaching rate of HA thin

nanoplates and nanorods is significantly higher than HA nanoplates. Such leaching behavior of HA nanorods, nanoplates, and thin nanoplates is directly related to their crystallinity, which was calculated to be ~ 89, 97 and 86 %, respectively. Higher crystalline nHA suggests lower dissolution ability [10-12].

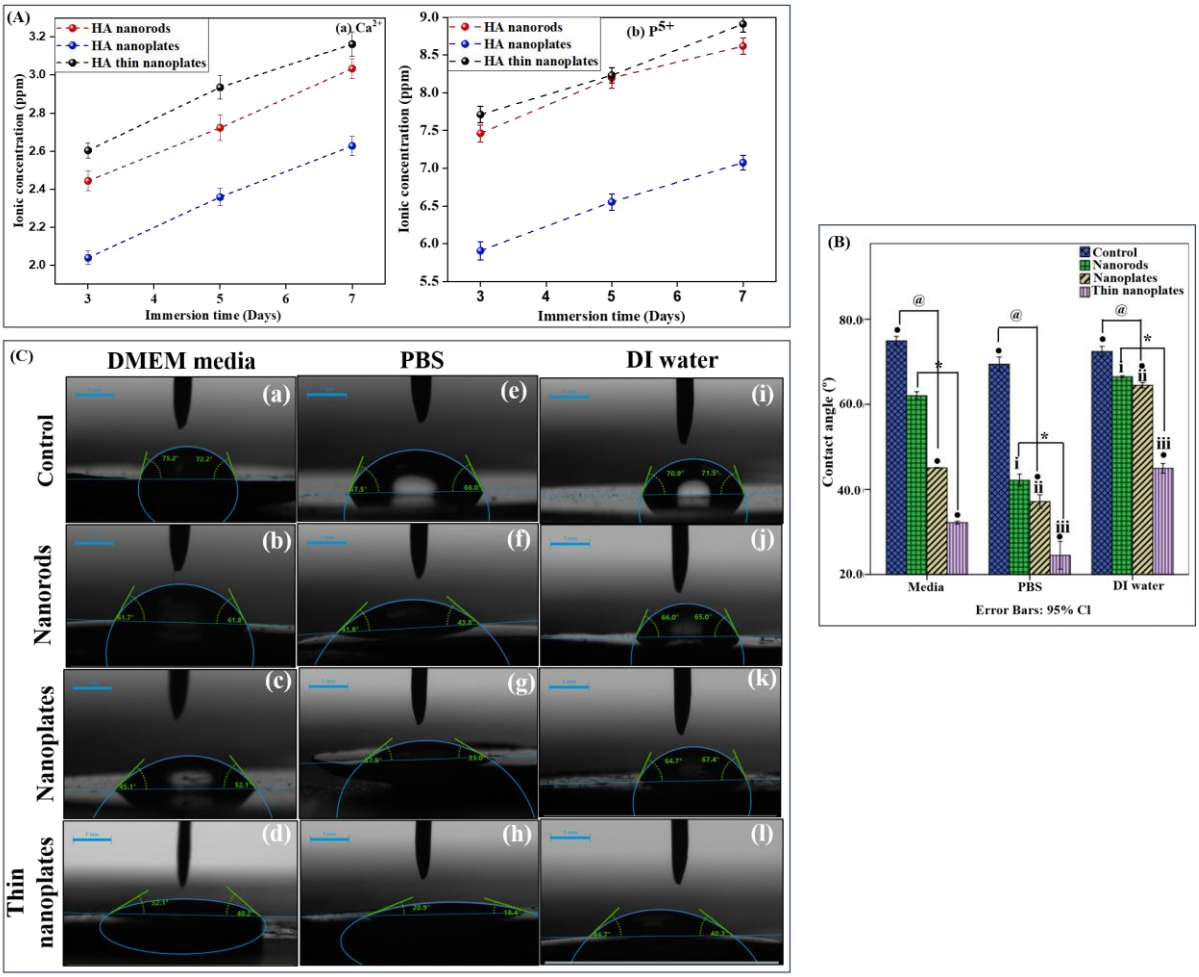

Figure 4.3. *(A) Ion release profile of Ca^{2+} (a) and P^{5+} (b) from HA nanorods, nanoplates, and thin nanoplates in simulated body fluid (SBF); and (B) Contact angle measurement of HA nanorods, nanoplates, thin nanoplates, and control in DI water, PBS and DMEM media. The mark (*) represents the statistically significant variation (at $p \leq 0.05$) in mean contact angle values on HA nanorods, nanoplates, thin nanoplates, with respect to control in all liquid media. The mark (●) indicates statistically significant variation (at $p \leq 0.05$) in mean contact angle values for HA nanoplates, thin nanoplates, and control as compared to HA nanorods. The mark*

(@) denotes the statistically significant variation (at $p \leq 0.05$) in mean contact angle value on HA nanorods, nanoplates, and control with respect to HA thin nanoplates. (C) Digital images, representing the contact angle measurement of HA nanorods, nanoplates, thin nanoplates, and control in DI water, PBS and DMEM media.

4.4. Contact angle measurement

The surface wettability of HA nanocrystals as per morphology (HA nanorods, nanoplates, and thin nanoplates) was assessed using contact angle measurement in various liquid solutions, such as DI water, PBS, and cell growth media with respect to glass coverslip as a control, as shown in Fig. 4.3B and C. Statistical analyses revealed that HA nanocrystals exhibited a significantly higher contact angle (indicating lower hydrophilicity) in DI water compared to growth media and PBS. Among the solutions, HA nanocrystals displayed the highest hydrophilicity in PBS, moderate in growth media, and lowest hydrophilicity in DI water. While assessing the contact angle as per morphology, the hydrophilicity of HA nanorods, nanoplates, and thin nanoplates increased sequentially across all liquids. Specifically, the contact angle reductions were observed as 39.29 %, 46.53 %, and 65 % in PBS and 17.29 %, 40 %, and 57.06 % in growth media for HA nanorods, nanoplates, and thin nanoplates, respectively, with respect to control. Finally, these results demonstrate that surface wettability of HA nanocrystals is morphological dependent with plate-like nanostructure exhibiting better hydrophilicity than rod-like one. This variation can be attributed to the difference in surface charge of HA nanorods (– 6.1 mV), nanoplates (–44.2 mV), and thin nanoplates (– 48.1 mV). A higher negatively-charged surface correlates with enhanced hydrophilicity [13]. Furthermore, surface oxygen vacancy also contributes to hydrophilicity through the adsorption of dissociative water molecules, leading to the formation of –OH groups on each oxygen vacancy. Such chemisorbed –OH groups enhance the interaction (Vander walls and hydrogen) between H_2O and – OH, which consequently improves the hydrophilicity [14-16]. The degree of hydrophilicity of HA

nanorods, nanoplates, and thin nanoplates is similar in order to their number of oxygen vacancies, which is in agreement with XPS result.

4.5. Hemocompatibility

Hemocompatibility assesses how well materials interact with RBCs with minimal or no adverse reaction. In order to investigate the biocompatibility of HA nanocrystals, the hemolysis assay was performed, which evaluates the amount of hemoglobin, released from raptured RBCs when exposed to HA samples. Fig. 4.4 depicts the percentage of hemolysis of RBCs after interaction with different morphologies of HA nanocrystals; nanorods, nanoplates, and thin nanoplates at concentrations of 0.2, 2 and 20 mg/ml. The results show that the hemolysis (%) gradually increases with increasing the nHA concentration from 0.2 to 2 mg/ml for all the morphologies, followed by a sharp increase when the concentration reaches 20 mg/ml. At concentrations of 0.2 and 2 mg/ml, the hemolysis for HA nanorods, nanoplates, and thin nanoplates is (1.2, 0.7 and 1.1 %) and (1.6, 1.6, and 1.5 %), respectively. In these cases, lysis of RBCs is less than 2 %, indicating the non-hemolytic property of HA nanorods, nanoplates, and thin nanoplates at concentrations of 0.2 and 2 mg/ml. Even at a concentration of 20 mg/ml, the hemolysis is 4.6, 3.7, and 4.2 % for all respective nHA morphologies, which remained under 5 %, i.e., hemocompatible as per ASTM-F756-00 standard. Specifically, HA nanorods damage a higher number of RBCs than HA nanoplates and thin nanoplates. Moreover, HA nanoplates show the lowest RBC damage at a concentration of 20 mg/ml. Such significant variation in hemolysis (%) as per nHA shape is related to surface charge, crystallinity, and release of Ca^{2+} ions. The surface charge on HA nanorods, nanoplates and thin nanoplates were calculated to be – 6.1, – 44.2 and – 48.1 mV. Less negative surface charge of HA nanorods means a more positively-charged surface. Thereby, it interacts more strongly with RBCs (negatively charged), leading to larger destruction of cell membrane than HA nanoplates and thin nanoplates [17]. Despite of the highest surface charge, HA thin nanoplates lyse a larger number of RBCs as compared

to nanoplates. Less crystalline HA thin nanoplates possess better dissolution ability than HA nanoplates, which, in turn, release more concentration of Ca^{2+} ions, as confirmed by ICP-MS experiments. The elevated concentration of Ca^{2+} ions exerts a high-pressure gradient inside and outside of RBCs due to osmotic shock. Through such pressure gradient, Ca^{2+} ions enter the RBCs and activate the Ca^{2+}-dependent K^+ channel (Gardos channel) that efflux K^+ ions. It facilitates the loss of intracellular fluid, which results in the RBCs shrinkage and potential hemolysis of RBCs [18, 19].

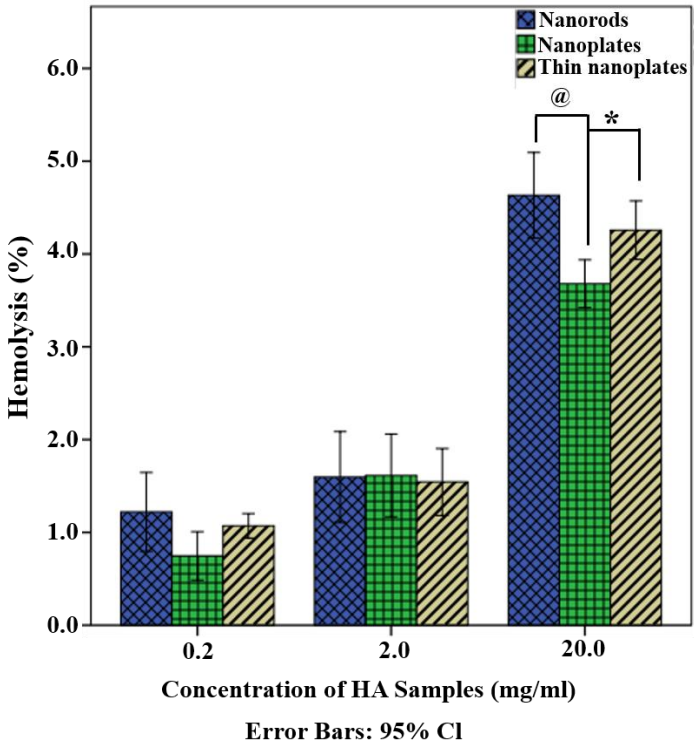

Figure 4.4. *Comparative assessment of hemolysis on HA nanorods, nanoplates, and thin nanoplates. The mark (*) represents the significant difference (at $p \leq 0.05$) in the mean value of hemolysis (%) on nanoplates and thin nanoplates as compared to HA nanorods. The mark (@) indicates the statistically significant variation (at $p \leq 0.05$) in mean values of hemolysis (%) on HA nanorods and nanoplates as compared to thin nanoplates.*

4.6. Cellular response

4.6.1. Cell viability evaluation

The viability of MG-63 cells on different morphological HA nanocrystals at various concentrations of 0.2, 2 and 20 mg/ml was quantitatively evaluated using MTT assay for 3, 5 and 7 culture days (Fig. 4.5). Statistical analyses demonstrated that all the nHA morphologies; HA nanorods, nanoplates, and thin nanoplates exhibit significantly higher cell viability as compared to control after 3 days of incubation. However, no significant variation in cell viability was observed among the various nHA concentrations and their respective morphologies. With continuous incubation for 5 days, cell viability in the control group has increased by 59.6 % with no considerable enhancement in cell viability on 0.2 and 2 mg/ml concentrated HA nanorods, nanoplates, and thin nanoplates. Even, cell viability on HA nanorods and thin nanoplates at concentrations of 0.2 and 2 mg/ml was slightly reduced. On similar incubation periods (5 days), the cell viability of MG-63 cells, treated with higher concentration, i.e., 20 mg/ml of nHA, appreciably increased by 45.1, 94.2 and 19.1 % (with respect to 3 culture days) for HA nanorods, nanoplates and thin nanoplates. HA nanoplates possess significantly higher cell viability than HA nanorods and thin nanoplates. On incubating the cells with nHA samples up to 7 days, the cell viability on HA nanorods, nanoplates, and thin nanoplates further increased by (132.8, 153 and 60 %), (156, 71 and 52 %), and (50.5, 29.3 and 21 %) at concentrations of 0.2, 2 and 20 mg/ml, respectively. The lower cell viability was observed at 2 mg/ml concentrated nHA compared to 0.2 and 20 mg/ml. In addition, HA nanoplates exhibit higher cell viability than HA nanorods, thin nanoplates and control at all concentrations. HA thin nanoplates revealed the lowest cell viability (even as compared to the control sample) with no considerable variation among their concentrations. These results suggest that HA nanoplates promote cell growth and proliferation more effectively than HA

nanorods and HA nanoplates. The high cell proliferation on HA nanorods is also observed, which is intermediate to HA nanoplates and thin nanoplates.

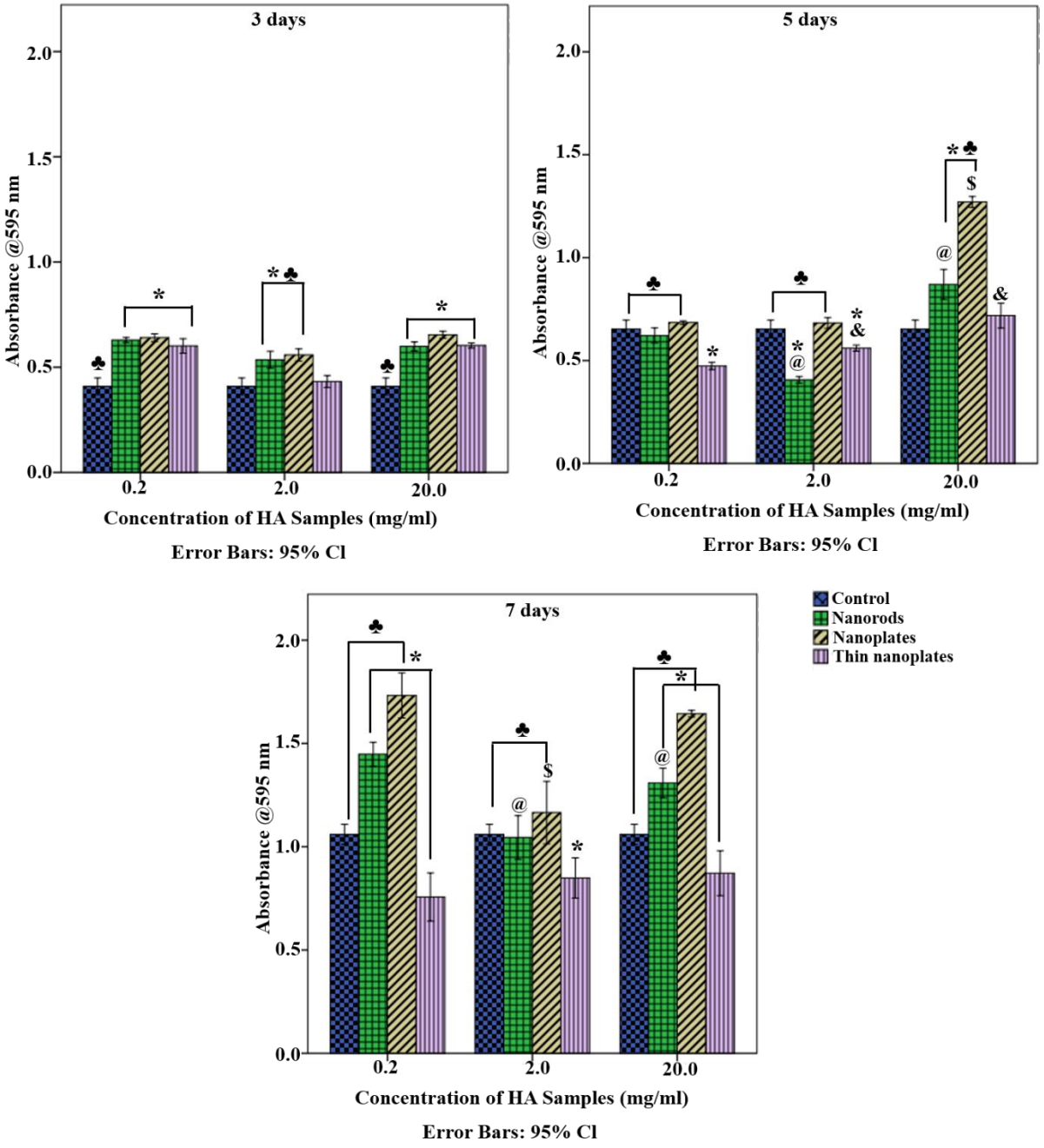

Figure 4.5. *Viability of MG-63 cells on different concentrations (0.2, 2 and 20 mg/ml) of HA nanorods, nanoplates, thin nanoplates, and control samples for 3, 5, and 7 culture days. The mark (*) denotes the statistically significant variation (at $p \leq 0.05$) in mean values of optical density of HA nanorods, nanoplates, and thin nanoplates, with respect to control at all*

concentrations. The marks (@) and ($) indicate statistically significant variation (at $p \leq 0.05$) in mean values of optical density of HA nanorods and nanoplates among the different concentrations, respectively.

4.6.2. Cell adhesion

The adhesion of MG-63 cells on HA nanorods, nanoplates, and thin nanoplates at different concentrations (0.2, 2 and 20 mg/ml) was analyzed depending on the spreading area and morphology of adhered cells after 3 days of incubation (Fig. 4.6). From Fig. 4.6A, cells adhered on the control surface exhibit an elongated and polygonal shape. The spreading of cells is observed to be higher in the case of HA nanorods, and nanoplates at a concentration of 0.2 mg/ml as compared to the control. However, HA thin nanoplates at the same concentration show less elongated and nearly round-shape cell morphology. It indicates a smaller spreading area for HA thin nanoplates than HA nanorods and nanoplates (Fig. 4.6B). As the concentration of nHA increases from 0.2 to 2 mg/ml, the spreading area of cells on HA nanorods and nanoplates decreases. Specifically, least cell adhesion is observed on the surface of HA nanorods as compared to HA nanoplates and thin nanoplates. A further increase in the concentration of HA nanocrystals from 2 to 20 mg/ml supported the cell adhesion. The spreading area of cells enhanced on HA nanorods and nanoplates. Specifically, HA nanoplates show larger, more elongated, and flattened cell morphology. It has a significantly higher spreading area than HA nanorods and thin nanoplates. The highest cell density is observed on HA nanoplates (20 mg/ml). These results demonstrate that HA nanoplates at a concentration of 20 mg/ml better support cell adhesion and proliferation.

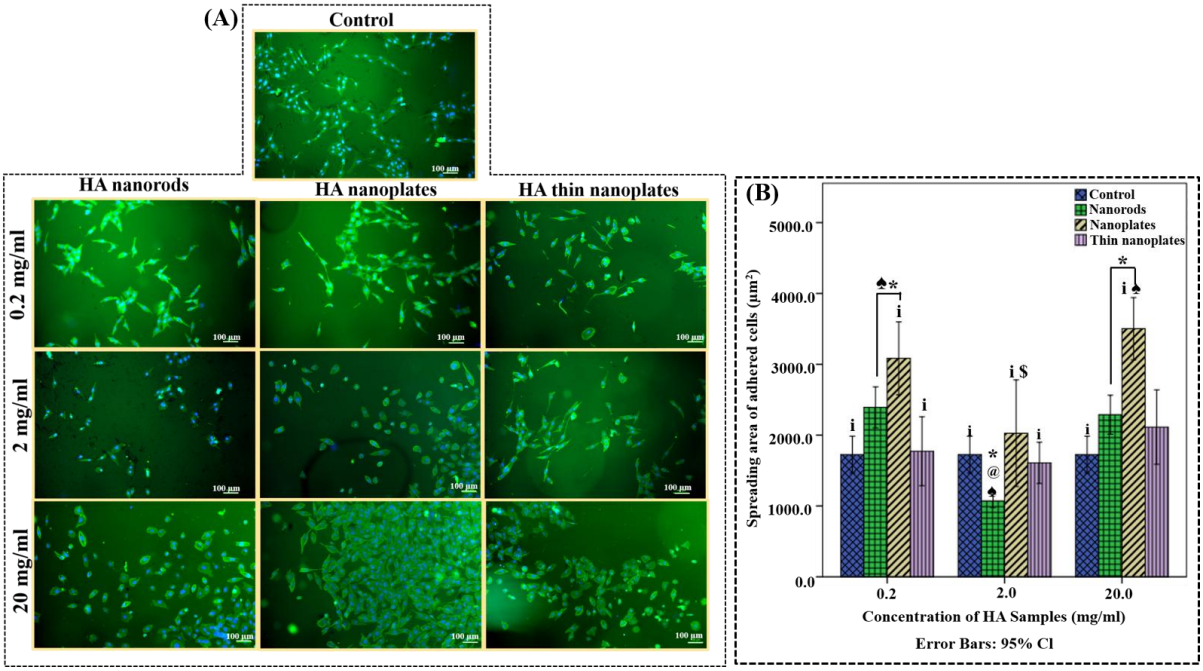

Figure 4.6. (A) *Qualitative cellular assessment of MG-63 cells at different concentrations (0.2, 2 and 20 mg/ml) of HA nanorods, nanoplates, thin nanoplates as well as control samples after 3 days of incubation (Scale bar: 100 µm); and (B) Spreading area of MG-63 cells, adhered on control, HA nanorods, nanoplates, and thin nanoplates.*

4.6.3. Osteogenic differentiation

Fig. 4.7 represents the ALP expression of MG-63 cells exposed to various concentrations (0.2, 2 and 20 mg/ml) of HA nanorods, nanoplates, and thin nanoplates over periods of 7 and 14 days. Statistical analyses found that after 7 days, the ALP activity of all similar morphologies of HA nanocrystals at concentrations of 0.2 and 2 mg/ml was lower than that of the control group. An increase in concentration from 2 to 20 mg/ml resulted in a significant rise in ALP expression for HA nanorods and nanoplates compared to the control, except HA thin nanoplates. ALP activity also varied among different shapes of nHA. At 0.2 mg/ml concentration, ALP activity of HA nanorods is 143.6 and 380 % higher than HA nanoplates and thin nanoplates, respectively, which possess no considerable variation among them at nHA concentration of 2 mg/ml. In contrast, at 20 mg/ml, HA nanoplates showed 13 and 103 %

higher ALP expression than HA nanorods and thin nanoplates. The HA thin nanoplates showed lower ALP activity at all nHA concentrations. After a continuous incubation for 14 days, ALP expression on the control surface was reduced with an absorbance value from 0.59 to 0.09. However, on varying the incubation period from 7 to 14 days, ALP activity on HA nanorods, nanoplates, and thin nanoplates drastically enhanced. The ALP expressions on respective nHA morphologies are similar in order, as observed in 7 days of incubation. Overall, 0.2 mg/ml concentrated HA nanorods and 20 mg/ml concentrated HA nanoplates represent excellent ALP activity. It indicates that HA nanorods (0.2 mg/ml) and HA nanoplates (20 mg/ml) significantly enhance the osteogenic differentiation of MG-63 cells compared to other concentrations of HA nanocrystals. As a result, they have the potential to promote new bone formation.

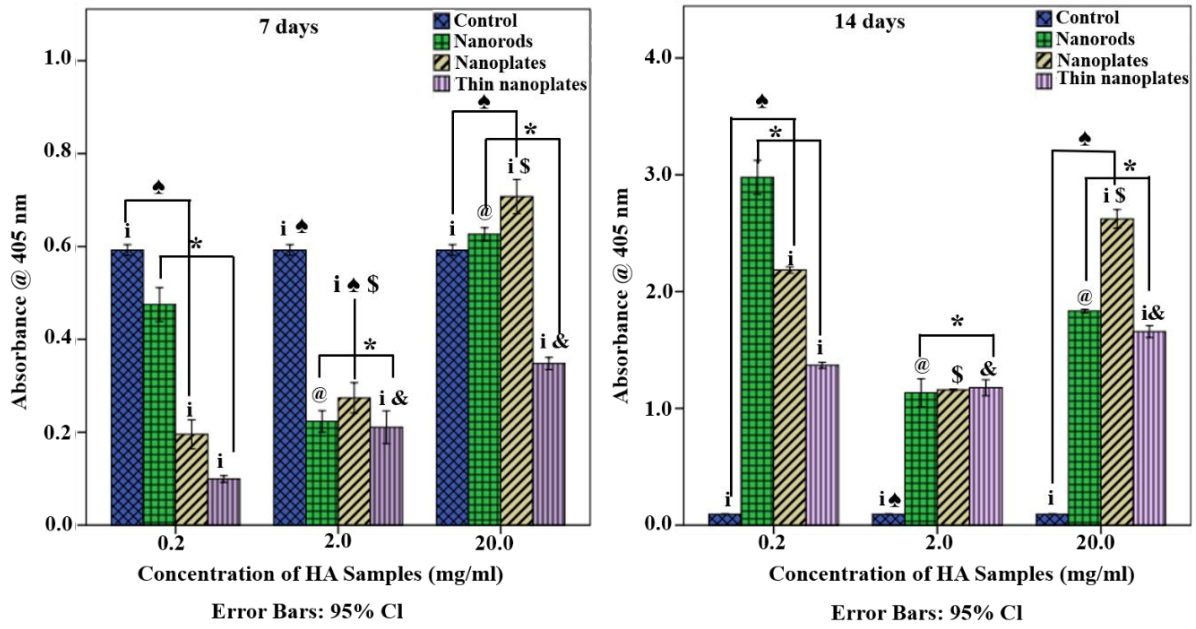

Figure 4.7. *The ALP expression of MG-63 osteoblast cells on HA nanorods, nanoplates, and thin nanoplates at concentrations of 0.2, 2 and 20 mg/ml, for 7 and 14 culture days. The asterisk (*) indicates a statistically significant variation (at $p \leq 0.05$) in mean absorbance values of HA nanorods, nanoplates, and thin nanoplates with respect to control at all concentrations. The mark (i) indicates the statistically significant variation (at $p \leq 0.05$) in HA nanoplates, thin nanoplates, and control as compared to HA nanorods. The mark (♠) represents the statistically*

significant variation (at $p \leq 0.05$) in HA nanorods, nanoplates, and control with respect to HA thin nanoplates. The marks (@), ($) and (&) indicate the statistically significant variation (at $p \leq 0.05$) in HA nanorods, nanoplates, and thin nanoplates among the different concentrations, respectively.

4.7. Discussion

In cell culture experiments, both quantitative and qualitative results showed that HA nanoplates enhance osteoblast cell adhesion and proliferation more effectively than HA nanorods and thin nanoplates across all nHA concentrations (0.2, 2, and 20 mg/ml). Such significant variation in cellular response of various shapes of HA nanocrystals seems to depend on several factors, such as surface charge, hydrophilicity, and released ions. The zeta potential measurement reveals that surface charges on HA nanorods, nanoplates, and thin nanoplates are – 6.1, – 44.2, and – 48.1 mV, respectively. It is possible that higher negatively-charged HA nanoplates initially interact electrostatically with number of cations, such as H^+, K^+, and Ca^{2+}, present in a biological fluid, which subsequently interacts with negatively-charged receptor proteins that facilitate cell adherence. In contrast, the comparatively lower negative charge on the surface of HA Nanorods attracts variety of anions (Cl^- and HPO_4^-) from the biological fluids. As a result, this diminishes the ability of negatively-charged receptor proteins to bind with the cells [20-22]. Naqshbandi [23] et al. suggested a similar mechanism, i.e., higher cell adhesion on a negatively-charged surface primarily dependent on the adsorption of surrounding cations. Another study also highlighted the positive impact of negatively-charged surfaces on the growth of osteoblast cells [24]. It is well-known that the hydrophilic surface also enhances the functions of bone cells, such as cell adhesion, proliferation, and growth [25-28]. The contact angle measurements demonstrated the degree of hydrophilicity in DMEM media. HA thin nanoplates exhibited the highest hydrophilicity, While HA nanoplates and nanorods showed moderate and lowest hydrophilicity, respectively. Interestingly, despite of highest zeta

potential and hydrophilicity, HA thin nanoplates demonstrated the lowest cytocompatibility. According to previous reports, elevated concentrations of extracellular Ca^{2+} ions induce a toxic effect on cell growth and proliferation. An et al.[29] reported the 4.22 % apoptotic rate for human dental cells after 24 h of incubation with 9 mM Ca^{2+} ions. Jaworska et al.[30], recently, revealed 30 % reduction in viability of MC3T3 osteoblast-like cells after 2 h of exposure to extracellular Ca^{2+} ions at a concentration of 6.25 mM. Palepšienė et al.[31] observed the slight decrease in cell viability even at 0.01 mM of extracellular Ca^{2+} ions The optimal concentration of intracellular Ca^{2+} ions plays an essential role in cell growth, proliferation, and regulating the cellular metabolism. To maintain the optimal condition of intracellular Ca^{2+} ions, the extracellular Ca^{2+} concentration is ~ 1 mM [32]. In our study, ICP-MS data revealed the leaching behavior of Ca^{2+} ions from nHA samples. HA thin nanoplates released the highest concentration of Ca^{2+} ions into biological fluids, while HA nanorods and nanoplates released moderate and the lowest amounts, respectively. The concentration of released Ca^{2+} ions from HA nanoplates is insufficient to disturb the optimal concentrations (1 mM) of extracellular Ca^{2+} ions. However, the Ca^{2+} ions released from HA nanorods and thin nanoplates can exceed the extracellular concentration of Ca^{2+} ions over the intracellular concentrations. In this condition, Ca^{2+} ions influx into the cytoplasm from the extracellular microenvironment through a calcium channel in the cell plasma membrane. Such a rise in cytosolic Ca^{2+} ions concentrations allows the Ca^{2+} ions to influx into mitochondria, where it disturbs the normal metabolic process that leads to cell death (Fig. 4.8) [32, 33]. The concentration of Ca^{2+} released from HA thin nanoplates is even higher than HA nanorods. As a result, HA thin nanoplates showed the lowest cytocompatibility.

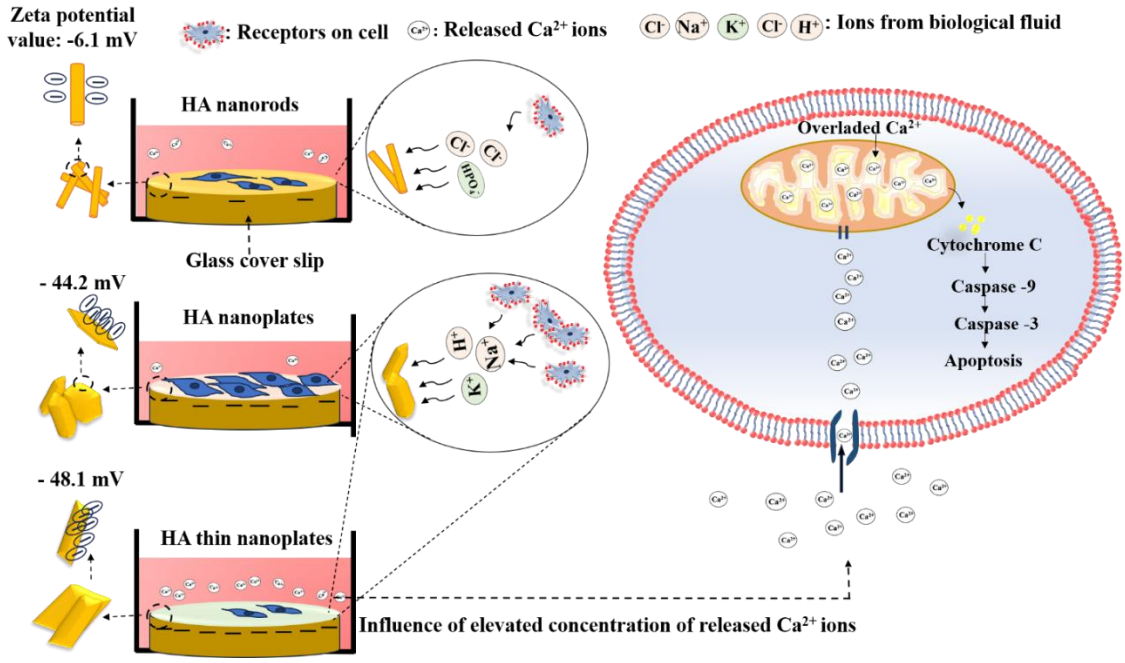

Figure 4.8. *The schematic diagram, illustrating the effect of surface charge and release of calcium ions on the cellular response of HA nanocrystals.*

ALP activity test revealed that the osteogenic differentiation of MG-63 cells was influenced by both concentrations and the morphology of nHA samples. HA nanorods exhibited the highest osteogenic activity at a low (0.2 mg/ml) concentration of HA nanocrystals. In contrast, HA nanoplates showed the highest osteogenic activity at a high concentration of 20 mg/ml. Additionally, HA thin nanoplates displayed the lowest osteogenic activity at all concentrations. At low concentrations, the size of HA nanocrystals seems to play a predominant role in the osteogenic differentiation of MG-63 cells. The size of HA nanorods and nanoplates were measured to be ~ 70 – 500 nm and 200 – 500 nm, respectively. However, HA thin nanoplates are of micrometers in size. Shi et al.[34] suggested that smaller-sized particles can more easily enter within cells, where they are digested by lysosomes and release Ca^{2+} ions in cytoplasm. Such a concentration of cytosolic Ca^{2+} ions favours osteogenic differentiation [34, 35]. Their study showed a stronger osteogenic response with smaller HA nanocrystals (20 nm) than larger ones. Yang et al.[36] also reported the similar effects of particle size on osteogenic

differentiation of osteoblast cells. This data aligns with our result of higher osteogenic activity in HA nanorods compared to larger-sized HA nanoplates and thin nanoplates. On increasing the concentration of nHA from 0.2 mg/ml to 2 and 20 mg/ml, agglomeration of nHA particles increases. Unlike the size of HA nanocrystals, surface charge and ion release can synergistically play a dominant role at 20 mg/ml concentration of HA nanocrystals, which stimulates the osteogenic differentiation of osteoblast cells on HA nanoplates better than that of HA nanorods and thin nanoplates. In addition, surface oxygen vacancies also positively affect osteogenesis phenomenon by acting the active sites for the adsorption of hydroxyl ions. Few research studies demonstrated that such hydroxyl ions are essential for CaP deposition, stimulating osteogenic differentiation [37, 38]. The higher number of hydroxyl ions enhances the adsorption of Ca^{2+} and PO_4^{3-} ions, leading to improved biomineralization. Our XPS data revealed the concentrations of oxygen vacancies in order— HA nanorods < HA nanoplates < HA thin nanoplates. Consequently, HA nanoplates exhibited better osteogenic activity than HA nanorods. The osteogenic differentiation of HA thin nanoplates should be higher as compared to HA nanorods and HA nanoplates due to their higher oxygen vacancy concentration. However, they showed the lowest osteogenic activity at all concentrations, which ascribed to elevated release of Ca^{2+} ions from HA thin nanoplates than HA nanorods and nanoplates. Such concentrations of Ca^{2+} inhibited the osteogenic differentiation [39, 40]. These findings are supported by previous study, reported by Zhang et al. [41]. Overall, HA nanoplates show superior cell adhesion, proliferation, and osteogenic differentiation as compared to HA nanorods and thin nanoplates. This indicates that HA nanoplates exhibit good biocompatibility and osteogenic activity. Such bone-mimicking morphology of HA nanocrystals can be a potential breakthrough biomaterial for bone tissue engineering applications.

References

[1] A. Diez-Escudero, M. Espanol, M.-P. Ginebra, High-aspect-ratio nanostructured hydroxyapatite: towards new functionalities for a classical material, Chemical Science 15(1) (2024) 55-76.

[2] P.R. Dev, C.P. Anand, D.S. Michael, P. Wilson, Hydroxyapatite coatings: a critical review on electrodeposition parametric variations influencing crystal facet orientation towards enhanced electrochemical sensing, Materials Advances 3(21) (2022) 7773-7809.

[3] J.-J. Guan, B. Tian, S. Tang, Q.-F. Ke, C.-Q. Zhang, Z.-A. Zhu, Y.-P. Guo, Hydroxyapatite coatings with oriented nanoplate arrays: synthesis, formation mechanism and cytocompatibility, Journal of Materials Chemistry B 3(8) (2015) 1655-1666.

[4] G. Bharath, B.S. Latha, E.H. Alsharaeh, P. Prakash, N. Ponpandian, Enhanced hydroxyapatite nanorods formation on graphene oxide nanocomposite as a potential candidate for protein adsorption, pH controlled release and an effective drug delivery platform for cancer therapy, Analytical Methods 9(2) (2017) 240-252.

[5] V.J. Huerta, P. Fernández, V. Gómez, O.A. Graeve, M. Herrera, Defect-related luminescence properties of hydroxyapatite nanobelts, Applied Materials Today 21 (2020) 100822.

[6] K. Shu, C. Chuaicham, Y. Noguchi, L. Xu, K. Sasaki, In-situ hydrothermal synthesis of Fe-doped hydroxyapatite photocatalyst derived from converter slag toward xanthate photodegradation and Cr(VI) reduction under visible-light irradiation, Chemical Engineering Journal 459 (2023) 141474.

[7] H. Wang, L. Zhao, X. Yu, S. Lei, Y. Qi, C. Cui, Synthesis of silver modified hydroxyapatite nanoparticle and evaluation of its biological properties in vitro for potential biomedical application, Journal of the Ceramic Society of Japan 129(7) (2021) 443-452.

[8] S. Wu, J. Wang, Q. Li, Z. Huang, Z. Rao, Y. Zhou, Bi/BiOCl Nanosheets Enriched with Oxygen Vacancies to Enhance Photocatalytic CO2 Reduction, Transactions of Tianjin University 27(2) (2021) 155-164.

[9] A. Arenas-Hernandez, C. Zuñiga Islas, M. Moreno, W. Calleja Arriaga, J.C. Mendoza-Cervantes, N. Carlos, C.R. Ascencio-Hurtado, A. Heredia Jiménez, Study of Oxygen Vacancies in TiO2 Nanostructures and Their Relationship with Photocatalytic Activity, Applied Sciences, 2022.

[10] R. Schneider, J. Kerkhoff, A. Danzer, A. Mattusch, A. Ohmann, M. Thommes, G. Sadowski, The interplay of dissolution, solution crystallization and solid-state transformation of amorphous indomethacin in aqueous solution, International Journal of Pharmaceutics: X 2 (2020) 100063.

[11] L. Zhang, T. Lu, F. He, W. Zhang, X. Yuan, X. Wang, J. Ye, Physicochemical and cytological properties of poorly crystalline calcium-deficient hydroxyapatite with different Ca/P ratios, Ceramics International 48(17) (2022) 24765-24776.

[12] W. Xue, X. Liu, X. Zheng, C. Ding, Effect of hydroxyapatite coating crystallinity on dissolution and osseointegration in vivo, Journal of Biomedical Materials Research Part A 74A(4) (2005) 553-561.

[13] Z. Zhuang, T.J. Fujimi, M. Nakamura, T. Konishi, H. Yoshimura, M. Aizawa, Development of a,b-plane-oriented hydroxyapatite ceramics as models for living bones and their cell adhesion behavior, Acta Biomaterialia 9(5) (2013) 6732-6740.

[14] D. Kuscer, J. Kovač, M. Kosec, R. Andriesen, The effect of the valence state of titanium ions on the hydrophilicity of ceramics in the titanium–oxygen system, Journal of the European Ceramic Society 28(3) (2008) 577-584.

[15] H. Hu, H.-F. Ji, Y. Sun, The effect of oxygen vacancies on water wettability of a ZnO surface, Physical Chemistry Chemical Physics 15(39) (2013) 16557-16565.

[16] F. Orudzhev, A. Muslimov, Oxygen Vacancies and Surface Wettability: Key Factors in Activating and Enhancing the Solar Photocatalytic Activity of ZnO Tetrapods, 24(22) (2023).

[17] X. Zhao, D. Lu, Q.S. Liu, Y. Li, R. Feng, F. Hao, G. Qu, Q. Zhou, Hematological Effects of Gold Nanorods on Erythrocytes: Hemolysis and Hemoglobin Conformational and Functional Changes, 4(12) (2017) 1700296.

[18] L. Kuck, J.N. Peart, M.J. Simmonds, Calcium dynamically alters erythrocyte mechanical response to shear, Biochimica et Biophysica Acta (BBA) - Molecular Cell Research 1867(11) (2020) 118802.

[19] Y. Zhang, Y. Xu, S. Zhang, Z. Lu, Y. Li, B. Zhao, The regulation roles of Ca2+ in erythropoiesis: What have we learned?, Experimental Hematology 106 (2022) 19-30.

[20] A.K. Dubey, B. Basu, Pulsed Electrical Stimulation and Surface Charge Induced Cell Growth on Multistage Spark Plasma Sintered Hydroxyapatite-Barium Titanate Piezobiocomposite, Journal of the American Ceramic Society 97(2) (2014) 481-489.

[21] M. Ohgaki, T. Kizuki, M. Katsura, K. Yamashita, Manipulation of selective cell adhesion and growth by surface charges of electrically polarized hydroxyapatite, Journal of biomedical materials research 57(3) (2001) 366-73.

[22] D. Khare, P. Singh, A.K. Dubey, Interplay of surface polarization charge, dynamic electrical stimulation and compositional modification towards accelerated osteogenic response of NaxK1-xNbO3 piezo-bioceramics, Biomaterials Advances 140 (2022) 213042.

[23] A. Naqshbandi, A. Rahman, Synthesis and characterization of chlorinated hydroxyapatite as novel synthetic bone substitute with negative zeta potential, Ceramics International 48(6) (2022) 8112-8117.

[24] S. Bodhak, S. Bose, A. Bandyopadhyay, Role of surface charge and wettability on early stage mineralization and bone cell–materials interactions of polarized hydroxyapatite, Acta Biomaterialia 5(6) (2009) 2178-2188.

[25] P. Singh, A.K. Dubey, Accelerated Osteogenic Response of Electrodynamically Stimulated Mg(1-x)Ca(x)Si(1-x)Zr(x)O(3) (x = 0-0.4) Bioelectrets, 9(11) (2023) 6293-6308.

[26] H. Ehtesabi, F. Massah, Improvement of hydrophilicity and cell attachment of polycaprolactone scaffolds using green synthesized carbon dots, Materials Today Sustainability 13 (2021) 100075.

[27] J. Guan, J. Wang, F. Jia, W. Jiang, L. Song, L. Xie, H. Yang, P. Han, H. Lin, Z. Wu, X. Zhang, Y. Huang, Layer-by-layer self-assembly coatings on strontium titanate nanotubes with antimicrobial and anti-inflammatory properties to prevent implant-related infections, Colloids and Surfaces B: Biointerfaces 244 (2024) 114183.

[28] F. Jia, D. Xu, Y. Sun, W. Jiang, H. Yang, A. Bian, Y. Liu, K. Liu, S. Zhang, Y. Wang, H. Qiao, H. Lin, J. Lan, Y. Huang, Strontium-calcium doped titanium dioxide nanotubes loaded with GL13K for promotion of antibacterial activity, anti-Inflammation, and vascularized bone regeneration, Ceramics International 49(22, Part B) (2023) 35703-35721.

[29] S. An, Y. Gao, Y. Huang, X. Jiang, K. Ma, J. Ling, Short-term effects of calcium ions on the apoptosis and onset of mineralization of human dental pulp cells in vitro and in vivo, International journal of molecular medicine 36(1) (2015) 215-21.

[30] K. Jaworska, J.J. Senior, A. Brüning-Richardson, A.M. Smith, The effect of elevating extracellular CaCl2: Important considerations for tissue engineering applications, Tissue and Cell 91 (2024) 102615.

[31] R. Palepšienė, M. Maciulevičius, P. Ruzgys, B. Jakštys, S. Šatkauskas, The Influence of Calcium Ions on the Electrotransfer Efficiency of Plasmid DNA and Cell Viability, Applied Sciences, 2023.

[32] A. Danese, S. Leo, A. Rimessi, M.R. Wieckowski, F. Fiorica, C. Giorgi, P. Pinton, Cell death as a result of calcium signaling modulation: A cancer-centric prospective, Biochimica et Biophysica Acta (BBA) - Molecular Cell Research 1868(8) (2021) 119061.

[33] G. Ermak, K.J. Davies, Calcium and oxidative stress: from cell signaling to cell death, Molecular immunology 38(10) (2002) 713-21.

[34] Z. Shi, X. Huang, Y. Cai, R. Tang, D. Yang, Size effect of hydroxyapatite nanoparticles on proliferation and apoptosis of osteoblast-like cells, Acta Biomater 5(1) (2009) 338-45.

[35] S. Maeno, Y. Niki, H. Matsumoto, H. Morioka, T. Yatabe, A. Funayama, Y. Toyama, T. Taguchi, J. Tanaka, The effect of calcium ion concentration on osteoblast viability, proliferation and differentiation in monolayer and 3D culture, Biomaterials 26(23) (2005) 4847-4855.

[36] X. Yang, Y. Li, X. Liu, R. Zhang, Q. Feng, In Vitro Uptake of Hydroxyapatite Nanoparticles and Their Effect on Osteogenic Differentiation of Human Mesenchymal Stem Cells, 2018 (2018) 2036176.

[37] M. Yu, J. Gong, Y. Zhou, L. Dong, Y. Lin, L. Ma, W. Weng, K. Cheng, H. Wang, Surface hydroxyl groups regulate the osteogenic differentiation of mesenchymal stem cells on titanium and tantalum metals, Journal of Materials Chemistry B 5(21) (2017) 3955-3963.

[38] Y. Yu, T. Wu, L. Dong, Surface Oxygen Vacancies of Rutile Nanorods Accelerate Biomineralization, ACS Omega 8(22) (2023) 20066-20072.

[39] Y. Han, High concentrations of calcium suppress osteogenic differentiation of human periodontal ligament stem cells in vitro, Journal of dental sciences 16(3) (2021) 817-824.

[40] Y.K. Liu, Q.Z. Lu, R. Pei, H.J. Ji, G.S. Zhou, X.L. Zhao, R.K. Tang, M. Zhang, The effect of extracellular calcium and inorganic phosphate on the growth and osteogenic differentiation of mesenchymal stem cells in vitro: implication for bone tissue engineering, Biomedical materials (Bristol, England) 4(2) (2009) 025004.

[41] W. Zhang, H. He, Y. Tian, Q. Gan, J. Zhang, Y. Yuan, C. Liu, Calcium ion-induced formation of β-sheet/-turn structure leading to alteration of osteogenic activity of bone morphogenetic protein-2, Sci Rep 5 (2015) 12694.